

RESEARCH ARTICLE

10.1002/2017MS001004

Lifen Jiang and Zheng Shi contributed equally to this work.

Key Points:

- A traceability framework is developed to trace the components of transient carbon storage dynamics
- The transient traceability framework can be applied to trace the differences in components of carbon storage dynamics in different ecosystems
- Different mechanisms are revealed by the framework to account for the similar trajectory of carbon storage dynamics in the two contrasting ecosystems

Supporting Information:

- Supporting Information S1

Correspondence to:

L. Jiang,
Lifen.Jiang@nau.edu;
Z. Shi,
zheng.shi@ou.edu;
Y. Luo,
Yiqi.Luo@nau.edu

Citation:

Jiang, L., Shi, Z., Xia, J., Liang, J., Lu, X., Wang, Y., & Luo, Y. (2017). Transient traceability analysis of land carbon storage dynamics: Procedures and its application to two forest ecosystems. *Journal of Advances in Modeling Earth Systems*, 9, 2822–2835. <https://doi.org/10.1002/2017MS001004>

Received 4 APR 2017

Accepted 30 OCT 2017

Accepted article online 8 NOV 2017

Published online 4 DEC 2017

© 2017. The Authors.

This is an open access article under the terms of the Creative Commons Attribution-NonCommercial-NoDerivs License, which permits use and distribution in any medium, provided the original work is properly cited, the use is non-commercial and no modifications or adaptations are made.

Transient Traceability Analysis of Land Carbon Storage Dynamics: Procedures and Its Application to Two Forest Ecosystems

Lifen Jiang¹ , Zheng Shi² , Jianyang Xia³, Junyi Liang^{2,4}, Xingjie Lu¹, Ying Wang⁵, and Yiqi Luo^{1,6}

¹Center for Ecosystem Science and Society, Northern Arizona University, Flagstaff, AZ, USA, ²Department of Microbiology and Plant Biology, University of Oklahoma, Norman, OK, USA, ³School of Ecological and Environmental Sciences, East China Normal University, Shanghai, China, ⁴Environmental Science Division and Climate Change Science Institute, Oak Ridge National Laboratory, Oak Ridge, TN, USA, ⁵Department of Mathematics, University of Oklahoma, Norman, Oklahoma, USA, ⁶Department of Earth System Science, Tsinghua University, Beijing, China

Abstract Uptake of anthropogenically emitted carbon (C) dioxide by terrestrial ecosystem is critical for determining future climate. However, Earth system models project large uncertainties in future C storage. To help identify sources of uncertainties in model predictions, this study develops a transient traceability framework to trace components of C storage dynamics. Transient C storage (X) can be decomposed into two components, C storage capacity (X_c) and C storage potential (X_p). X_c is the maximum C amount that an ecosystem can potentially store and X_p represents the internal capacity of an ecosystem to equilibrate C input and output for a network of pools. X_c is codetermined by net primary production (NPP) and residence time (τ_N), with the latter being determined by allocation coefficients, transfer coefficients, environmental scalar, and exit rate. X_p is the product of redistribution matrix (τ_{ch}) and net ecosystem exchange. We applied this framework to two contrasting ecosystems, Duke Forest and Harvard Forest with an ecosystem model. This framework helps identify the mechanisms underlying the responses of carbon cycling in the two forests to climate change. The temporal trajectories of X are similar between the two ecosystems. Using this framework, we found that different mechanisms lead to a similar trajectory between the two ecosystems. This framework has potential to reveal mechanisms behind transient C storage in response to various global change factors. It can also identify sources of uncertainties in predicted transient C storage across models and can therefore be useful for model intercomparison.

1. Introduction

Terrestrial ecosystem carbon (C) dynamic is one of key components that determine future climate since terrestrial ecosystems can uptake a substantial fraction of the important greenhouse gas, carbon dioxide (CO₂) emissions by anthropogenic activities. Land has sequestered approximately one-third CO₂ emissions from fossil fuels and cement and land use change during 2004–2013 (Le Quéré et al., 2015). However, several model intercomparison projects (MIPs) have demonstrated large uncertainty in the projections of terrestrial C dynamics by land surface models (LSMs). For example, Tian et al. (2015) reported substantial differences in estimated contemporary global soil C stocks ranging from 425 to 2111 Pg C by 10 terrestrial biosphere models in the Multi-scale Synthesis and Terrestrial Model Intercomparison Project (MsTMIP); Todd-Brown et al. (2014) showed large differences in modeled soil C stock changes ranging from a loss of 72 Pg to a gain of 253 Pg C in the next 100 years by the Earth system models (ESMs) involved in Coupled Model Intercomparison Project Phase 5 (CMIP5).

Great effort has been made to identify the causes of model uncertainty among ESMs. For example, climatic forcing from the general circulation models (GCMs) explains the majority of uncertainties in the projected 21st century terrestrial C balance by a dynamic global vegetation model (Ahlström et al., 2013); using a reduced complexity model, Todd-Brown et al. (2013) found that differences in the simulated soil C across CMIP5 ESMs can be explained by net primary production (NPP) and the parameterization of soil heterotrophic respiration; C residence time is responsible for the major uncertainties in the modeled vegetation or soil C storage by LSMs or CMIP5 ESMs (Friend et al., 2014; He et al., 2016; Jiang et al., 2015; Wang et al., 2011).

Even though these processes or parameters have been identified to be responsible for model uncertainty, systematical analysis across models is lacking and remains challenging for model improvement due to the low practicability (Fisher et al., 2014). In addition, more and more processes are incorporated into LSMs or ESMs, which makes identifying sources of model uncertainty even more difficult.

Shared properties among most land C cycling models make systematical analysis possible (Luo et al., 2015, 2016). Using a traceability framework, Xia et al. (2013) successfully traced the difference in ecosystem carbon storage capacity among different biomes to four model components: NPP, baseline C residence times, environmental scalars, and climate forcing. As most LSMs share the same model structures, this traceability framework has the potential to help diagnose the sources of uncertainties in LSM projections of C storage. For example, it has been applied to a global vegetation model, LPJ-GUESS, to trace ecosystem C cycle processes and to evaluate the importance of vegetation dynamics for future terrestrial C cycling (Ahlström et al., 2015).

The traceability framework proposed by Xia et al. (2013) was developed to trace C storage capacity of an ecosystem under steady state. It is even more important to understand future terrestrial C storage dynamics (i.e., transient state). In order to reduce uncertainties in model projections, we need to understand responses of C storage dynamics to future climate and other global change factors and the underlying mechanisms. Recently, Luo et al. (2017) conducted a theoretical analysis on the determinants of transient C storage dynamics, by adding another term, C storage potential, to the steady state traceability framework developed by Xia et al. (2013). C storage potential represents instantaneous C pool size at a time step at which disturbances such as temperature and precipitation prevent the actual C storage of an ecosystem away from its maximum C capacity if the ecosystem keeps at equilibrium at that time (Luo et al., 2017). The theoretical analysis on transient C storage dynamics has potential applications in several different ways, among which are to explore the mechanisms underlying the responses of ecosystem C cycle to climate change and to identify the sources of model uncertainties to improve model performance for more reliable predictions of future C storage status.

In addition to evaluate uncertainty among models, the transient traceability framework can also be applied to different simulated ecosystems to identify the difference of the components of the framework. While Luo et al. (2017) focused on mathematical foundation of the transient framework, this study explores its application by providing step-by-step details to carry out the analysis and by comparing different components of the framework in two different ecosystem types. Specifically, the transient traceability framework is explored with the Terrestrial Ecosystem (TECO) model in two contrasting ecosystems, Duke needleleaved forest and Harvard deciduous broadleaved forest. We investigate how the traceable components of transient C storage dynamics responded to the rising CO₂ and climate change in the two contrasting ecosystem types.

2. Materials and Methods

2.1. The Transient Traceability Framework: Technical Details

This study proposes a traceability framework to trace modeled transient C storage dynamics of terrestrial ecosystems, which is based on the theoretical analysis on transient C dynamics by Luo et al. (2017) and the steady state traceability framework on C storage capacity by Xia et al. (2013).

It has well been documented that ordinary differential equations that characterize C movements from one pool to another in most terrestrial C cycle models can be represented by a matrix formula (Luo et al., 2017; Manzoni & Porporato, 2009; Sierra & Müller, 2015; Xia et al., 2013):

$$X'(t) = B(t)u(t) - A\zeta(t)KX(t) \quad (1)$$

where $X'(t)$ is net change of any individual C pool at time t , which is a vector for a multipool model, and the sum of X' of all individual C pools is net ecosystem production (NEP) or negative net ecosystem exchange (NEE); $B(t)$ is a vector of allocation coefficients of C input to each pool; $u(t)$ is C input, i.e., NPP or gross primary production (GPP); A is a matrix of transfer coefficients between C pools; $\zeta(t)$ is a diagonal matrix of environmental scalars to reflect the control of physical and chemical properties, e.g., temperature, moisture, nutrients, litter quality and soil texture, on C cycle processes; and K is a diagonal matrix of exit rates from donor pools, which is mortality rates for plant pools and decomposition coefficients for litter and soil pools; and $X(t)$ is individual pool size at time t , which is also a vector in a multipool model (Luo et al., 2017; Xia et al., 2013). For example, in the TECO model (Luo et al., 2016; Shi et al., 2015; Weng & Luo, 2008), which

has eight carbon pools (leaf, wood, root, litter, coarse wood debris, and fast, slow, and passive soil organic matter (SOM) pools, supporting information Figure S1) with feedback between the three soil C pools, the vector B , matrix A , and diagonal matrices ξ and K are as follows, respectively:

$$B(t) = \begin{pmatrix} b_1(t) \\ b_2(t) \\ b_3(t) \\ 0 \\ 0 \\ 0 \\ 0 \\ 0 \end{pmatrix}$$

where $b_1(t)$, $b_2(t)$, and $b_3(t)$ are allocation coefficients of NPP to pool 1 (leaf), pool 2 (wood), and pool 3 (root), respectively.

$$A = \begin{pmatrix} 1 & 0 & 0 & 0 & 0 & 0 & 0 & 0 \\ 0 & 1 & 0 & 0 & 0 & 0 & 0 & 0 \\ 0 & 0 & 1 & 0 & 0 & 0 & 0 & 0 \\ -a_{41} & -a_{42} & -a_{43} & 1 & 0 & 0 & 0 & 0 \\ 0 & -a_{52} & 0 & 0 & 1 & 0 & 0 & 0 \\ 0 & 0 & 0 & -a_{64} & -a_{65} & 1 & -a_{67} & -a_{68} \\ 0 & 0 & 0 & 0 & -a_{75} & -a_{76} & 1 & 0 \\ 0 & 0 & 0 & 0 & 0 & -a_{86} & -a_{87} & 1 \end{pmatrix}$$

where a_{ij} is a transfer coefficient from pool j to i , for example, a_{41} is the coefficient for C transferred from pool 1 (leaf) to 4 (litter), and so on.

$$\xi(t) = \begin{pmatrix} \xi_1(t) & 0 & 0 & 0 & 0 & 0 & 0 & 0 \\ 0 & \xi_2(t) & 0 & 0 & 0 & 0 & 0 & 0 \\ 0 & 0 & \xi_3(t) & 0 & 0 & 0 & 0 & 0 \\ 0 & 0 & 0 & \xi_4(t) & 0 & 0 & 0 & 0 \\ 0 & 0 & 0 & 0 & \xi_5(t) & 0 & 0 & 0 \\ 0 & 0 & 0 & 0 & 0 & \xi_6(t) & 0 & 0 \\ 0 & 0 & 0 & 0 & 0 & 0 & \xi_7(t) & 0 \\ 0 & 0 & 0 & 0 & 0 & 0 & 0 & \xi_8(t) \end{pmatrix}$$

$$K = \begin{pmatrix} k_1 & 0 & 0 & 0 & 0 & 0 & 0 & 0 \\ 0 & k_2 & 0 & 0 & 0 & 0 & 0 & 0 \\ 0 & 0 & k_3 & 0 & 0 & 0 & 0 & 0 \\ 0 & 0 & 0 & k_4 & 0 & 0 & 0 & 0 \\ 0 & 0 & 0 & 0 & k_5 & 0 & 0 & 0 \\ 0 & 0 & 0 & 0 & 0 & k_6 & 0 & 0 \\ 0 & 0 & 0 & 0 & 0 & 0 & k_7 & 0 \\ 0 & 0 & 0 & 0 & 0 & 0 & 0 & k_8 \end{pmatrix}$$

And the matrix $A\xi(t)K$ can be derived as follows:

$$A\xi(t)K = \begin{pmatrix} \xi_1(t)k_1 & 0 & 0 & 0 & 0 & 0 & 0 & 0 \\ 0 & \xi_2(t)k_2 & 0 & 0 & 0 & 0 & 0 & 0 \\ 0 & 0 & \xi_3(t)k_3 & 0 & 0 & 0 & 0 & 0 \\ -\xi_1(t)k_1a_{41} & -\xi_2(t)k_2a_{42} & -\xi_3(t)k_3a_{43} & \xi_4(t)k_4 & 0 & 0 & 0 & 0 \\ 0 & -\xi_2(t)k_2a_{52} & 0 & 0 & \xi_5(t)k_5 & 0 & 0 & 0 \\ 0 & 0 & 0 & -\xi_4(t)k_4a_{64} & -\xi_5(t)k_5a_{65} & \xi_6(t)k_6 & -\xi_7(t)k_7a_{67} & -\xi_8(t)k_8a_{68} \\ 0 & 0 & 0 & 0 & -\xi_5(t)k_5a_{75} & -\xi_6(t)k_6a_{76} & \xi_7(t)k_7 & 0 \\ 0 & 0 & 0 & 0 & 0 & -\xi_6(t)k_6a_{86} & -\xi_7(t)k_7a_{87} & \xi_8(t)k_8 \end{pmatrix}$$

By letting equation (1) equal zero, Xia et al. (2013) developed a traceability framework to decompose steady state ecosystem C storage into four fundamental components. Luo et al. (2017) further analyzed the determinants and the characteristics of transient dynamics of terrestrial C storage based on mathematical analysis of equation (1) with numeric examples. In detail, multiply both sides of equation (1) by $(A\xi(t)K)^{-1}$ and move $X(t)$ to the left-hand side, then equation (1) can be transformed to

$$X(t) = (A\xi(t)K)^{-1}B(t)u(t) - (A\xi(t)K)^{-1}X'(t) \tag{2}$$

The term $(A\xi(t)K)^{-1}$ in equation (2) is a matrix of C residence time through a network of individual pools. This matrix is named as redistribution matrix, $\tau_{ch}(t)$, which measures time needed for net C pool change to be redistributed in the network containing all C pools. The matrix of $\tau_{ch}(t)$ can be expressed as

$$(A\xi(t)K)^{-1} = \begin{pmatrix} \tau_1 & 0 & 0 & 0 & 0 & 0 & 0 & 0 \\ 0 & \tau_2 & 0 & 0 & 0 & 0 & 0 & 0 \\ 0 & 0 & \tau_3 & 0 & 0 & 0 & 0 & 0 \\ f_{41}\tau_4 & f_{42}\tau_4 & f_{43}\tau_4 & \tau_4 & 0 & 0 & 0 & 0 \\ 0 & f_{52}\tau_5 & 0 & 0 & \tau_5 & 0 & 0 & 0 \\ f_{61}\tau_6 & f_{62}\tau_6 & f_{63}\tau_6 & f_{64}\tau_6 & f_{65}\tau_6 & \tau_6 & f_{67}\tau_6 & f_{68}\tau_6 \\ f_{71}\tau_7 & f_{72}\tau_7 & f_{73}\tau_7 & f_{74}\tau_7 & f_{75}\tau_7 & f_{76}\tau_7 & (1-a_{68}a_{86})\tau_7 & f_{78}\tau_7 \\ f_{81}\tau_8 & f_{82}\tau_8 & f_{83}\tau_8 & f_{84}\tau_8 & f_{85}\tau_8 & f_{86}\tau_8 & f_{87}\tau_8 & (1-a_{67}a_{76})\tau_8 \end{pmatrix}$$

where the diagonal elements of the matrix $(A\xi(t)K)^{-1}$ measure C residence times (τ) of individual pools. The term, $a_{68}a_{86}$, is added to the seventh diagonal element to indicate the loop that does not go through pool 7 (slow SOM). Similarly, the term, $a_{67}a_{76}$, is added to the eighth diagonal element to reflect the loop that does not go through pool 8 (passive SOM). The nondiagonal elements measure residence times of a fraction of C transferred from pool j to i , f_{ij} , through all pathways as following:

$$\begin{aligned} f_{41} &= a_{41} \\ f_{42} &= a_{42} \\ f_{43} &= a_{43} \\ f_{52} &= a_{52} \\ f_{61} &= a_{64}a_{41} \\ f_{62} &= a_{64}a_{42} + (a_{65} + (a_{67} + a_{68}a_{87})a_{75})a_{52} \\ f_{63} &= a_{64}a_{43} \\ f_{64} &= a_{64} \\ f_{65} &= a_{65} + (a_{67} + a_{68}a_{87})a_{75} \\ f_{67} &= a_{67} + a_{68}a_{87} \\ f_{68} &= a_{68} \\ f_{71} &= a_{76}a_{64}a_{41} \\ f_{72} &= a_{76}a_{64}a_{42} + (a_{76}a_{65} + a_{75} - a_{68}a_{75}a_{86})a_{52} \\ f_{73} &= a_{76}a_{64}a_{43} \\ f_{74} &= a_{76}a_{64} \\ f_{75} &= a_{76}a_{65} + a_{75} - a_{68}a_{75}a_{86} \\ f_{76} &= a_{76} \\ f_{78} &= a_{76}a_{68} \end{aligned}$$

$$\begin{aligned}
 f_{81} &= (a_{86} + a_{87}a_{76})a_{64}a_{41} \\
 f_{82} &= (a_{86} + a_{87}a_{76})a_{64}a_{42} + ((a_{86}a_{67} + a_{87})a_{75} + (a_{86} + a_{87}a_{76})a_{65})a_{52} \\
 f_{83} &= (a_{86} + a_{87}a_{76})a_{64}a_{43} \\
 f_{84} &= (a_{86} + a_{87}a_{76})a_{64} \\
 f_{85} &= (a_{86}a_{67} + a_{87})a_{75} + (a_{86} + a_{87}a_{76})a_{65} \\
 f_{86} &= a_{86} + a_{87}a_{76} \\
 f_{87} &= a_{86}a_{67} + a_{87}
 \end{aligned}$$

Multiplying $\tau_{ch}(t)$ by $B(t)$, the allocation coefficients, we can obtain C residence time of individual pools in the network, τ_N :

$$\tau_N(t) = (A\xi(t)K)^{-1}B(t) \tag{3}$$

Ecosystem C residence time, τ_E , is the sum of C residence time of all individual pools, τ_N . C storage capacity at time t is the product of C input (NPP or GPP) and C residence time (τ_N), and is defined as C storage capacity, X_c . The product of redistribution matrix, τ_{ch} , and net C pool change, X' , represents the redistribution of X' through the network containing all individual pools. It is an indicator of the potential of an ecosystem to sequester C (positive values) or release C (negative values) at time t and is named as C storage potential, X_p . Therefore, equation (2) can be rewritten as

$$X(t) = X_c(t) - X_p(t) \tag{4}$$

By incorporating the theoretical foundation above by Luo et al. (2017) on transient C storage dynamics into the existing traceability framework on steady state ecosystem C storage capacity by Xia et al. (2013), we propose a transient traceability framework to trace the components of transient C storage as shown in Figure 1. This transient traceability framework allows us not only to investigate transient C storage dynamics in response to rising CO₂, climate change, disturbances such as fire and drought, and land use change, etc., but also to understand the underlying mechanisms that cause the changes in C storage in a variable of ecosystems with ecosystem models or globally with LSMs or ESMs.

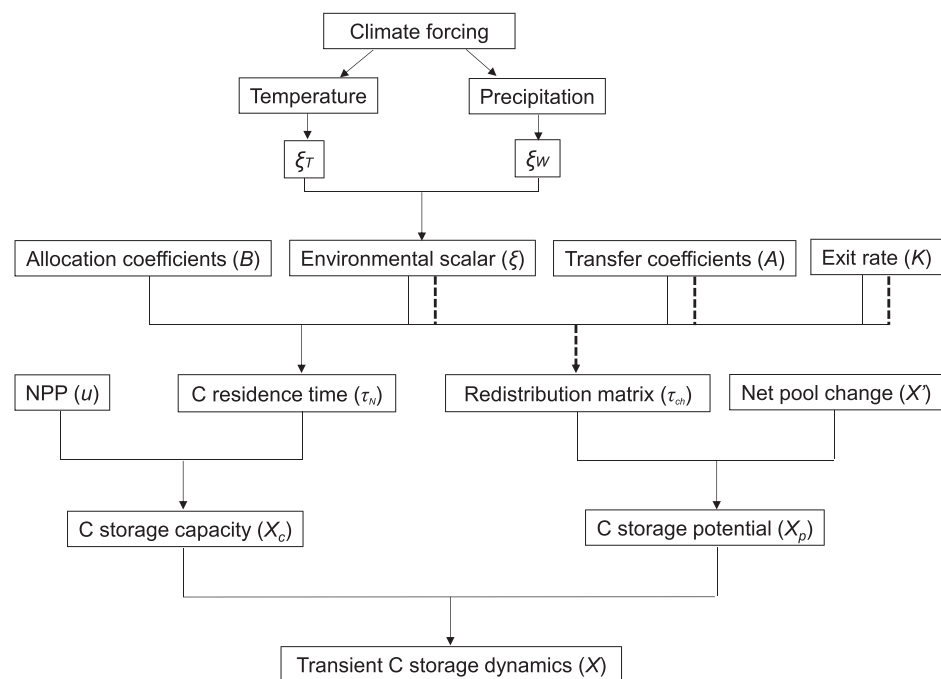


Figure 1. Schematic diagram of the traceability framework to analyze transient carbon storage dynamics of terrestrial ecosystems. ξ_W and ξ_T are water and temperature scalars, respectively. Dashed lines show the components that determine redistribution matrix (τ_{ch}).

2.2. The TECO Model

We explore this transient traceability framework with an ecosystem model, TECO model, to simulate C storage dynamics of Duke Forest and Harvard Forest in response to rising CO₂ and climate change from 1850 to 2100. The structure of TECO model is shown in supporting information Figure S1. It has eight C pools, which are three plant pools: leaf, wood, and root; litter; coarse wood debris; and three soil pools, consisting of fast, slow and passive SOM.

GPP is calculated using a canopy photosynthesis model embedded in the TECO model (Weng & Luo, 2008). In brief, leaf photosynthesis is estimated using the Farquhar photosynthesis model (Farquhar et al., 1980) and a stomatal conductance model (Ball et al., 1987). Leaf photosynthesis upscales to the canopy photosynthesis by a multilayer process-based model, which is mainly based on the model developed by Wang and Leuning (1998). Foliage is divided into sunlit and shaded leaves. It simulates radiation transmission in the canopy based on Beer's law.

A plant growth submodel simulates carbon allocation in TECO. Allocation of assimilated carbon among the leaves, stems, and roots depends on their growth rates. The plant growth submodel simulates plant growth rate by root/shoot ratio, scalar of NSC (nonstructural carbon), and a scalar of leaf area index. $G_i = G_{max_i} \times BM_i \times S_{r/s} \times S_{NSC} \times S_{LAI}$, where, $i = \text{leaf, stem, or root}$. G_i is the growth rate, G_{max_i} is the maximum relative growth rate, BM_i is the biomass of leaves, stems or roots. $S_{r/s}$, S_{NSC} , and S_{LAI} are the scaling factors derived from root/shoot ratio, the size of nonstructural carbon pool, and leaf area index, respectively. $b_i = G_i / \sum(G_i)$, where b_i is the allocation of NPP to leaf, stem or root.

The overall relationship among them is $GPP = Ra + NPP$ (aka $u(t)$) + NSC, where GPP is gross primary productivity, Ra is autotrophic respiration, NPP is net primary productivity, and NSC is nonstructural carbon in plants.

The decay of C pools is modified by environmental scalars. The environmental scalar is the product of temperature scalar (S_t) and moisture scalar (S_ω), with $S_t = Q_{10}^{(T_{soil}-0)/10}$ and $S_\omega = S_{w_min} + (1 - S_{w_min}) * Amin1$ (1.0, 2.0* ω). Q_{10} is temperature sensitivity, ω is the soil water content, and S_{w_min} is the permanent wilting point.

Photosynthesis, after deducting plant autotrophic respiration, i.e., NPP, is allocated to leaf, wood, and root with allocation coefficients of b_1 , b_2 , and b_3 , respectively. C in the three plant pools will enter either litter or coarse wood debris pool when plant organs die. C will transfer from one pool to another as indicated by the arrows in supporting information Figure S1 with transfer coefficients that are specific for the donor pools and the receiving pools. There are corresponding CO₂ fluxes resulting from plant respiration or decomposition of litter and SOM. Full description of the TECO model equations is available in Weng and Luo (2008, Appendix A).

2.3. Study Sites

The two ecosystems that we simulate, Duke Forest and Harvard Forest, are both temperate forests in U.S. but have distinct vegetation types. In addition, there are plenty of studies that have been done in these two forest ecosystems, making it more easily to parameterize and validate the TECO model. Duke Forest site is located in North Carolina, USA (35°58'41.41"N, 79°5'39.12"W) with a vegetation type of evergreen needle-leaf forests. Mean annual temperature of Duke Forest is 14.36°C and mean annual precipitation is 1,170 mm. The dominant tree species at this site is *Pinus taeda* (loblolly pine), which were planted in 1983 after a clear cut and a burn. There are some emergent *Liquidambar styraciflua* (sweetgum) in canopy. The understory consists of 26 woody species and diversity of the understory is still growing (AmeriFlux, 2016).

Being a deciduous broadleaf forest, Harvard Forest is located in Massachusetts, USA (42°32'16.08"N, 72°10'17.40"W) and has a much colder mean annual temperature of 6.62°C than Duke Forest and a similar mean annual precipitation of 1,071 mm with Duke Forest (AmeriFlux, 2016). Harvard Forest is dominated by *Quercus rubra* (red oak) and *Acer rubrum* (red maple) and was 75–110 years old in 2006 (Urbanski et al., 2007).

2.4. Implementation of the Transient Traceability Framework With TECO

Climate forcing data, including air and soil temperature, precipitation, photosynthetically active radiation, vapor-pressure deficit, and relative humidity, are derived from offline run of the Community Land Model 4.5

(CLM4.5, Oleson et al., 2013) for both historical (1850–2005) and RCP8.5 (2006–2100) simulations. Historical climate forcing data of CLM4.5 are CRUNCEP data set of which the missing values have been filled with Qian et al. (2006) data set according to the descriptions of CLM offline model forcing data at National Center for Atmospheric Research (http://www.cesm.ucar.edu/models/cesm1.2/clm/clm_forcingdata_esg.html). The above climate data in the grid where Duke Forest or Harvard Forest are located are extracted as forcing to drive the TECO model to simulate transient C storage dynamics from 1850 to 2100.

To calibrate the TECO model for simulating C storage dynamics at Duke Forest and Harvard Forest, GPP data by eddy flux measurements at Duke Forest during 2003–2006 and at Harvard Forest during 1997–2006 are downloaded from AmeriFlux website (<http://ameriflux.lbl.gov/>). After calibration, the agreements between the modeled GPP and the observed GPP from eddy flux measurements are good at both sites (supporting information Figure S2). Before running the TECO model for simulations from 1850 to 2100, climate forcing data of 10 years from 1850 to 1859 are recycled to spin up the TECO model to the equilibrium state in preindustrial environmental conditions. Then the model is driven by the climate data from 1850 to 2100 to simulate C dynamics for that time period. Variables that are needed for the transient traceability framework are output for analysis of transient C storage dynamics. That is, we use the matrix of the TECO model, i.e., equation (2), to calculate X , X_c , and X_p and further analyze how transient X , X_c , and X_p are determined by their components. The workflow for conducting the transient traceability analysis is summarized in supporting information Figure S3.

3. Results

3.1. Transient Ecosystem Carbon Storage Dynamics, Capacity, and Potential

The transient traceability framework works very well to simulate C storage dynamics in response to rising CO₂ and climate change (supporting information Figure S4). The transient traceability framework using matrix representation can derive almost identical ecosystem C storage with the direct model outputs for both Duke Forest and Harvard Forest. This allows further analysis of C storage dynamics and their components. In both Duke and Harvard Forests, transient C storage, X , is mostly determined by its maximum storage capacity, X_c , and C storage potential, X_p , only accounts for a small proportion of X_c (Figure 2a). As time progresses, the differences between X_c and X , i.e., X_p , become larger and larger in both ecosystems.

The trajectories of X , X_c , and X_p are very similar between Duke Forest and Harvard Forest. X , X_c , and X_p are all increasing over time, indicating that both Duke and Harvard Forests sequester more and more C from 1850 to 2100. X and X_c in Harvard Forest are systematically higher than those in Duke Forest. In detail, X and X_c are approximately 10 kg C m⁻² greater than those in Duke Forest. For example, mean X of last 10 year historical simulations (1996–2005) and last 10 year future projections (2091–2100) in Duke Forest are 18.46 and 24.89 kg C m⁻², respectively, and those values for Harvard Forest are 28.02 and 34.75 kg C m⁻², respectively. Mean X_c during the periods of 1996–2005 and 2091–2100 in Duke Forest are 19.35 and 27.50 kg C m⁻², respectively, whereas the corresponding X_c in Harvard Forest are 29.20 and 37.65 kg C m⁻², respectively. Different from X and X_c , X_p in the two ecosystems is close to each other.

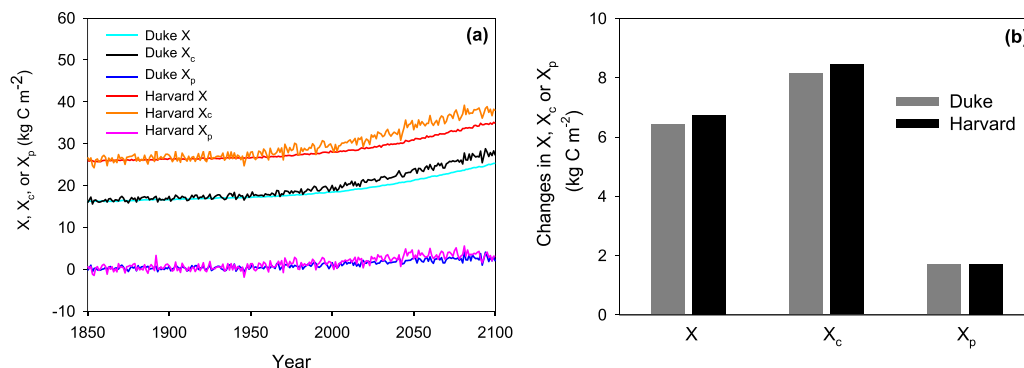


Figure 2. (a) Transient carbon storage (X), carbon storage capacity (X_c), and carbon storage potential (X_p) of the whole ecosystem in Duke and Harvard Forests and (b) their changes by the end of the 21st century.

Predicted changes in X by the end of the 21st century, that is, 10 year mean of X during 2091–2100 minus 10 year mean of X during 1996–2005, are a little higher in Harvard Forest than that in Duke Forest (6.73 versus 6.44 kg C m⁻², Figure 2b), which exactly follows the patterns of the changes in X_c : an increase of 8.45 kg C m⁻² in Harvard Forest versus an increase of 8.16 kg C m⁻² in Duke Forest. With increased X_p in both forests, the magnitudes of changes in X_p by the end of the 21st century are very similar between the two ecosystems.

3.2. Transient Carbon Storage Dynamics, Capacity, and Potential of Individual Pools

As ecosystem C storage dynamics, X of individual pools closely tracks X_c in the two ecosystems (Figure 3). X and X_c of all eight C pools in the two forests are increasing with time. X_p is small for most of the C pools in Duke and Harvard Forests, especially for leaf, root and litter pools so that X for these three pools is very close to X_c throughout the simulation period. Being increasing over time as well, the increments of X_p are also small in most C pools, but substantial increments occur in slow and passive soil C pools in both forests.

Given the different C amounts in individual pools between Duke Forest and Harvard Forest, the temporal patterns of X , X_c , and X_p of individual pools are very similar between the two ecosystems, except for a little difference in leaf and wood pools. In the deciduous broadleaf forest, Harvard Forest, leaf pool does not increase as much as that in the evergreen needleleaf forest, Duke Forest. Another noticeable phenomenon is that although X_p for leaf is very small in both Duke and Harvard Forests, the interannual variability of leaf pool in Duke Forest becomes larger and larger over time while the interannual variability of leaf pool in Harvard Forest is not as significant as that in Duke Forest. X , X_c , and X_p in wood in Harvard Forest are much higher than those in Duke Forest. Correspondingly, the increments of X , X_c , and X_p in wood are greater in Harvard Forest than in Duke Forest.

3.3. Net Primary Production and Ecosystem Carbon Residence Time

By decomposing X_c into NPP and C residence time, we find that NPP increases over time in both ecosystems and does not differ much between Duke Forest and Harvard Forest (Figure 4a). Unlike NPP, ecosystem C residence time of Harvard Forest is much longer than that of Duke Forest (Figure 4b), resulting in higher X_c in Harvard Forest than in Duke Forest (Figure 2a). Moreover, trajectories of C residence time show different trends between the two ecosystems. Specifically, C residence time in Duke Forest increases with time, whereas that in Harvard Forest decreases (Figure 4b). By the end of the 21st century, NPP increases by 0.55 and 0.42 kg C m⁻² yr⁻¹ in Duke Forest and Harvard Forest, respectively (Figure 4c), compared to those during the historical period. C residence time in Duke Forest increases by 0.29 year by the end of the 21st century but that in Harvard Forest decreases by 0.55 year.

3.4. Environmental Scalars

Environmental scalar, which represents control of temperature and precipitation on C residence time and redistribution matrix in this study, is higher in Duke Forest than that in Harvard Forest throughout the simulation period (Figure 5a). While environmental scalars in both Duke and Harvard Forests become greater and greater along the proceeding of time, indicating less and less limitations of temperature and moisture on soil C decomposition. Accordingly, residence time and redistribution matrix in both ecosystems are negatively affected. The increment of environmental scalar by the end of the 21st century in Harvard Forest is doubled of that in Duke Forest (Figure 5b).

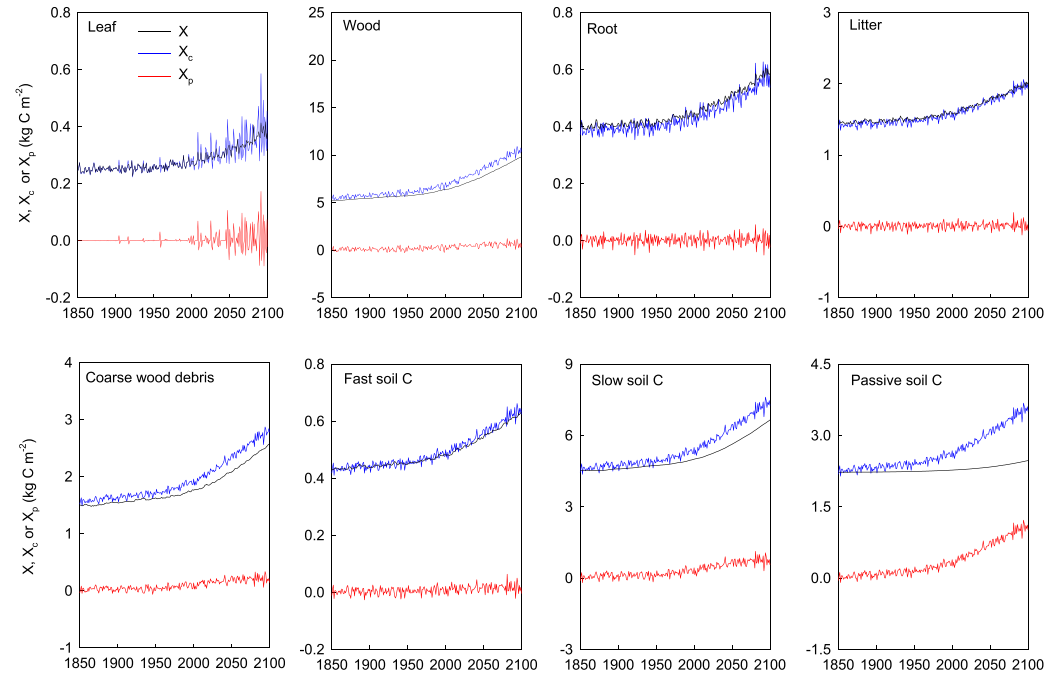
3.5. Allocation Coefficients

Allocation coefficients of NPP to leaf, wood and root, as represented by b_1 , b_2 , and b_3 in Figure 6a, exhibit different time courses between Duke Forest and Harvard Forest. In detail, allocation coefficients of NPP to leaf and root, i.e., b_1 and b_3 , in Duke Forest decrease over time, but allocation coefficient to wood, i.e., b_2 , is substantially enhanced. In Harvard Forest, in contrast, only allocation coefficient to root, b_3 , declines and those to leaf and wood, i.e., b_1 and b_2 , both increase. The changes in b_1 , b_2 , and b_3 by the end of the 21st century are characterized by a considerable decrease in b_1 and a dramatic increase in b_2 in Duke Forest (Figure 6b).

3.6. Redistribution Matrix and Net Ecosystem Production

As shown in equation (2) and Figure 1, C storage potential, X_p , is codetermined by redistribution matrix and net C pool change, X' , or at ecosystem scale, NEE or NEP. Figure 7 shows the correlation between X_p and

Duke Forest



Harvard Forest

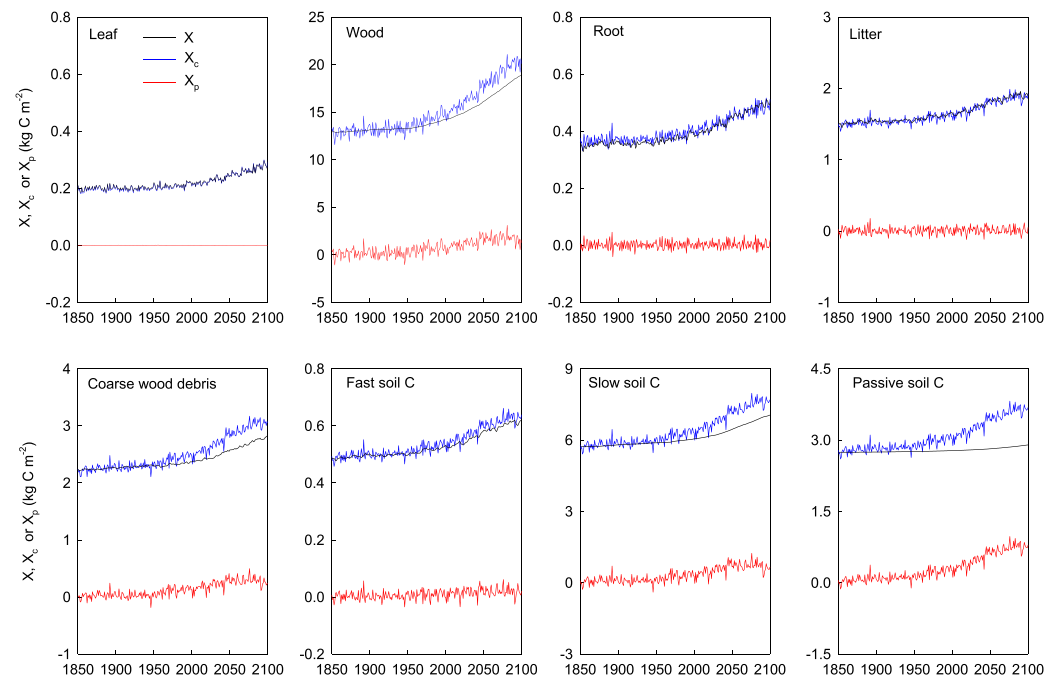


Figure 3. Transient carbon storage (X), carbon storage capacity (X_c), and carbon storage potential (X_p) of each carbon pool in Duke and Harvard Forests.

NEP. The correlation coefficients, R^2 , are high in both Duke Forest (0.80) and Harvard Forest (0.79). This indicates that, at a given place, X_p is mostly determined by NEP rather than redistribution matrix. Redistribution matrix, represented by the slopes of the linear regressions between X_p and NEP, is an indicator of an approximate time needed for ecosystem transient C storage to reach C storage capacity if current net ecosystem production and C storage capacity had been constant. Comparing between different places, X_p can

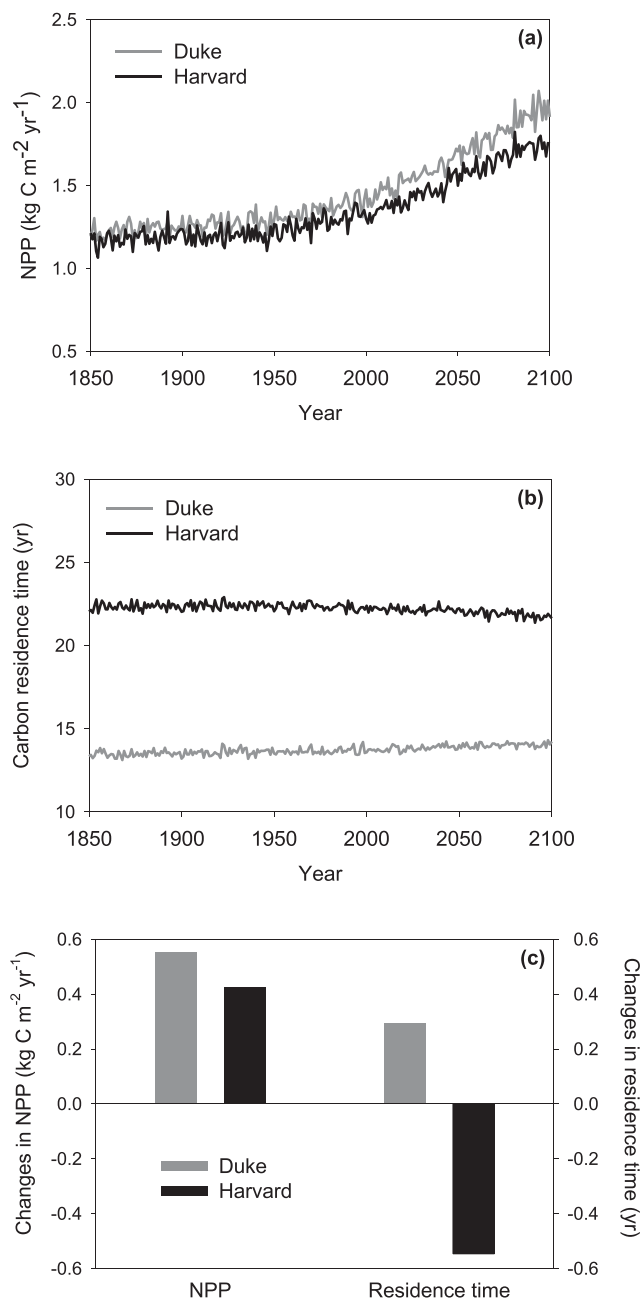


Figure 4. (a) Net primary production (NPP) and (b) ecosystem carbon residence time in Duke and Harvard Forests and (c) their changes by the end of the 21st century.

be influenced by redistribution matrix. According to Figure 7, having shorter redistribution matrix, X_p in Duke Forest is lower than that in Harvard Forest.

4. Discussion

Transient C storage dynamics are critical for predictions of future C storage status and therefore climate. Identifying sources in model-model uncertainties is required in order to improve model performance and better represent the reality. The theoretical analysis of transient C storage dynamics by Luo et al. (2017) provides the basis for extending the steady state traceability framework by Xia et al. (2013) to the transient traceability framework proposed in this study. The transient traceability framework (Figure 1) decomposes the transient C storage into C storage capacity and C storage potential, and both of them can be further decomposed into different components that are related to model parameters or climate forcing. We implement the transient traceability framework in the TECO model to simulate transient C storage dynamics from 1850 to 2100 in two forest ecosystems, Duke Forest and Harvard Forest. The framework works well as shown in supporting information Figure S4. With the transient traceability framework, we are able to track how each component of transient C storage responds to rising CO₂ and climate change in the two distinct ecosystems. Therefore, not only the dynamics of transient C storage are explored but also the mechanisms behind the different responses of the two ecosystems to CO₂ and climate change can be recognized.

4.1. Transient Carbon Storage Dynamics, Capacity, and Potential

Transient C storage can be decomposed into two major components, C storage capacity and C storage potential. By doing this, we can explore the differences in the responses of transient C storage dynamics to rising CO₂ and climate change in Duke and Harvard Forests. Although systematic differences in C pool size exist between Duke Forest and Harvard Forest due to the inherent differences in the two forests, there are many similarities in transient C storage, C storage capacity and C storage potential between the two ecosystems. For instance, X closely chases X_c , both increasing over time in the two ecosystems (Figure 2a), indicating that both Duke Forest and Harvard Forest will act as C sink until 2100. X_p accounts for a small proportion of X_c throughout the simulation period in both ecosystems. Moreover, X_p is always positive in this case study although theoretically it can be negative, i.e., C source, at any time (Luo et al., 2017).

Duke Forest and Harvard Forest will sequester more C under future atmospheric CO₂ concentration and climate. Our results are consistent with global terrestrial C storage projected by ESMs (Arora et al., 2013; Friedlingstein et al., 2014; Jones et al., 2013; Peng et al., 2014). In

ESMs, increasing C storage can be as a result of many covarying factors, e.g., rising CO₂, warmer temperature, dynamics of vegetation, land use change, and disturbances. However, in the present study, increase of C storage is mainly a product of elevated CO₂ and climate change because we did not explore how other factors may influence C storage dynamics.

Plants and soils in Duke Forest have been found to store more C under elevated CO₂ than ambient CO₂ according to the studies in the Free-Air Carbon dioxide Enrichment (FACE) experiment conducted in Duke Forest for 6–10 years (Lichter et al., 2005; McCarthy et al., 2010). In Harvard Forest, in situ observations

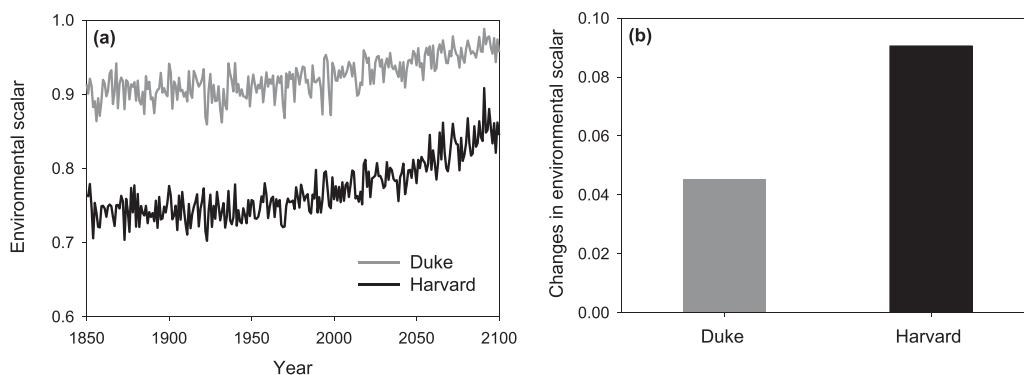


Figure 5. (a) Environmental scalar for carbon storage in Duke and Harvard Forests and (b) their changes by the end of the 21st century.

showed that C storage in wood and soils was both increasing with time (Barford et al., 2001; Urbanski et al., 2007). However, the results from the soil warming experiment conducted in Harvard Forest revealed that warming soil alone stimulated C gains in wood, but accelerated C losses from soils, resulting in a net C source from this ecosystem (Melillo et al., 2011). Due to the challenges in conducting factorial design of global change experiments, there is no experimental evidence on how C storage changes under combined elevated CO₂ and climate change in these two ecosystems.

4.2. Contrasting Mechanisms Underlying Transient Carbon Storage Dynamics Between Duke Forest and Harvard Forest

The response of X_c to elevated CO₂ and climate change is similar between Duke Forest and Harvard Forest (Figure 2a). However, the similar trajectories between the two ecosystems are actually as a result of different mechanisms: in Duke Forest, the two components of X_c , NPP and C residence time, both increase with time; in contrast, in Harvard Forest, NPP also increases over time as in Duke Forest, but its C residence time gradually decreases (Figure 4).

Simulated NPP often increases with elevated CO₂ and temperature (Friend et al., 2014; Sitch et al., 2008; Todd-Brown et al., 2014; Wieder et al., 2015). Our result is consistent with previous studies. C residence time was usually predicted to decline as a result of warmer temperature (Carvalhais et al., 2014; Todd-Brown et al., 2014). In this study, however, the TECO model simulates different trends of C residence time over time between Duke Forest and Harvard Forest. The differences can be explained by decomposing C residence time into its components. As shown in Figure 1, C residence time is determined by allocation coefficients, B , transfer coefficients, A , environmental scalar, ξ , and exit rate, K . In the TECO model, A and K are set as constants, but B varies with time. Therefore, time-varying ξ and B will be indicative for the differences in changes of C residence time between the two ecosystems. Decline of C residence time in Harvard Forest can be attributed to climate warming and changes in precipitation as reflected by the less and less limitations of environmental conditions on C turnover (Figure 5). ξ becomes higher and higher in both

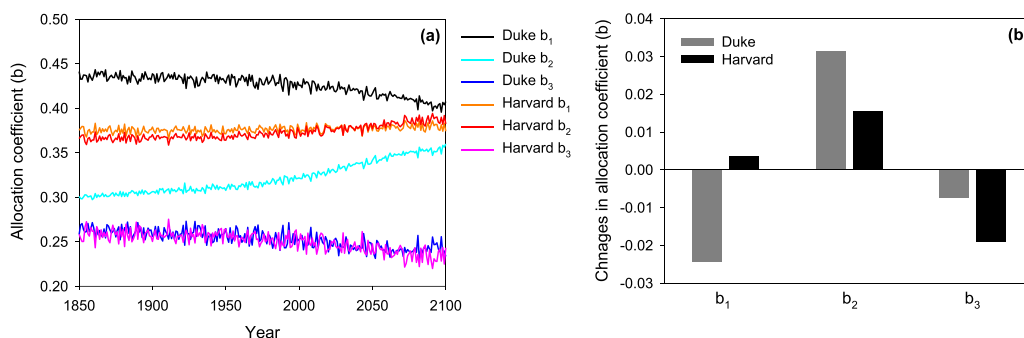


Figure 6. (a) Allocation coefficients of net primary production (NPP) to leaf (b_1), wood (b_2), and root (b_3) in Duke and Harvard Forests and (b) their changes by the end of the 21st century.

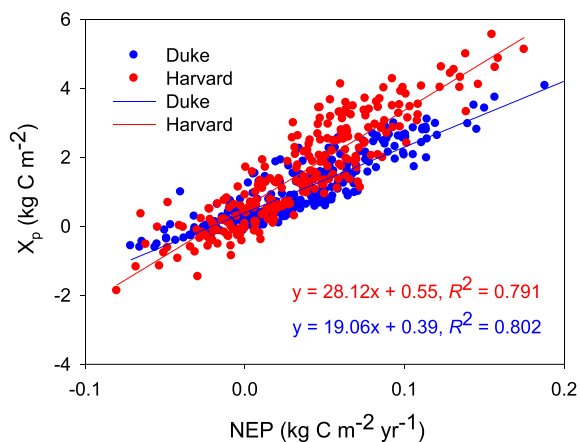


Figure 7. Correlation between net ecosystem production (NEP) and carbon storage potential (X_p) in Duke and Harvard Forests.

ecosystems and that means future climate will favor C turnover. The increment of ξ in Harvard Forest is much more than that in Duke Forest, and the substantial reduction of environmental limitations on C turnover in Harvard Forest may result in shorter residence time over time. Environmental scalars represent responses of C cycle to changes in climate (e.g., temperature and moisture), nutrients, litter quality, and soil texture (Luo et al., 2017). In this study, the environmental scalars only refer to control of climate (temperature and precipitation) on C residence time as we did not examine the effects of other factors.

Unlike in Harvard Forest, C residence time of Duke Forest increases over time although environmental scalar in Duke Forest also increases. The increase of C residence time in Duke Forest is a result of more allocation of NPP to wood. Ecosystem C residence time is the sum of C residence time of each C pool, therefore, changes in size of each C pool and their respective residence time will result in changes of ecosystem C residence time. In this study, modeled allocation of NPP to different plant pools, i.e., leaf, wood, and root, is found to respond to rising CO_2 and climate change differently between the two ecosystems. Significantly more NPP allocated to wood and much less NPP allocated to leaf in Duke Forest (Figure 6) may explain increased C residence time in this ecosystem since C resides longer through the pathway of wood than that of leaf. This result is coincided with an analysis on partitioning of NPP at FACE experiments in Duke Forest and three broadleaf forests, in which it concluded that the fraction of aboveground NPP partitioned to wood biomass was not enhanced by elevated CO_2 in the three broadleaf forests, whereas was enhanced in the conifer forest in Duke (McCarthy et al., 2006), but the changes in partitioning of C among plant pools in the Duke Forest FACE experiment could be caused by underestimation of allometrically determined plant biomass (McCarthy et al., 2010).

4.3. Implications of the Transient Traceability Framework and Future Research

The transient traceability framework extends the steady state traceability framework developed by Xia et al. (2013) to decompose transient C storage into different components. It works well to investigate the similarities and differences in transient C storage dynamics between Duke Forest and Harvard Forest. We have addressed how transient C storage dynamics will respond to rising CO_2 and climate change in the two ecosystems and are able to attribute the differences in transient C storage dynamics to different components with this transient traceability framework. In this case study, other than rising CO_2 and climate change, we did not explore how other global change factors such as N deposition, vegetation dynamics, land use change, and disturbance (e.g., fire, drought and insect breakout) influence transient C dynamics. Shift in disturbance regimes can also move ecosystem C storage toward a new dynamic disequilibrium (Luo & Weng, 2011). However, if an ecosystem model or an ESM simulates the effects of N deposition, vegetation dynamics, land use change, and disturbance, the application of the transient traceability framework to such a model can address those questions because those processes do not conflict with the assumptions on which the transient traceability framework is built (Luo et al., 2017).

It is no doubt that the ecosystem models can be run at multiple sites to compare more ecosystems. It can also be run under different scenarios for a specific ecosystem. Another potential application of the transient traceability framework is to implement it in an ESM to compare the differences in various biomes or under different scenarios. When it is applied to multiple ESMs such as in MIPs, the framework can help identify the causes for the uncertainties in transient C storage dynamics across models. A frustration faced by climate change research is that ESMs generate large uncertainties in their projections of future land C storage and this makes policy making to mitigate climate change a tough task. With the models becoming more and more complex, it is even more challenging to identify the causes for the uncertainties in model projections (Luo et al., 2015, 2016). Efforts have been made to identify the causes for the differences in model projections of C storage or uptake (e.g., Anav et al., 2013; Arora et al., 2013; Brovkin et al., 2013; Cox et al., 2013; Friedlingstein et al., 2006; Tian et al., 2015; Todd-Brown et al., 2013). These efforts contribute to help recognize the sources for the uncertainties across models. However, the lack of systematical analysis on model performance, which is due partly to the complex model structures and large numbers of parameters in

ESMs, impedes model improvements to reduce the uncertainties across models. Since the transient traceability framework tracks the model differences deeply into the specific processes or parameters, this would explicitly guide the modelers to improve their models. This framework using matrix representation will also enable data assimilation to be easily applied in ecosystem models or other complex models. Model projections of ecosystem models such as the TECO model (Shi et al., 2015) or complex models such as global land C models (Hararuk et al., 2014; Hararuk & Luo, 2014; He et al., 2016) have been substantially improved via data assimilation using matrix representation of these models. Data assimilation technique was recognized as the highest priority to improve predictions of soil C dynamics in ESMs (Luo et al., 2015). By combining with data assimilation to improve model performance, the transient traceability framework has potential to substantially reduce the uncertainties among ESMs and therefore to gain more reliable projections.

With the transient traceability framework, we quantified the C storage potential, X_p , in Duke Forest and Harvard Forest. X_p is novel in C cycle research and has never been quantified before the theoretical study by Luo et al. (2017). C storage potential represents the internal capacity of transient C storage to reach maximum C storage at equilibrium and it indicates the direction and rate of transient C movements at a time step (Luo et al., 2017).

5. Conclusions

The transient traceability framework we developed in this study can decompose modeled transient C storage dynamics in Duke Forest and Harvard Forest into two components, C storage capacity and C storage potential, both of which can be further decomposed and traced. With this framework, we are able to distinguish different responses of C storage dynamics between Duke Forest and Harvard Forest to rising CO₂ and climate change and the underlying mechanisms. This framework has potential to reveal the mechanisms behind transient C storage dynamics in response to various global change factors in different ecosystems. It can also help identify the sources of uncertainties in predicted transient C storage across models and, therefore, can be useful for model intercomparison and model improvement.

Acknowledgments

The data used in this study can be obtained at Yiqi Luo's lab website (<http://www2.nau.edu/luo-lab/download>) or by contacting the corresponding author Yiqi Luo (Yiqi.Luo@nau.edu). We thank Manoj KC for his help with forcing data from CLM4.5. This work was partially done through the working group, Nonautonomous Systems and Terrestrial Carbon Cycle, at the National Institute for Mathematical and Biological Synthesis, an institute sponsored by the National Science Foundation, the US Department of Homeland Security, and the US Department of Agriculture through NSF award EF-0832858, with additional support from the University of Tennessee, Knoxville. Research in Yiqi Luo EcoLab was financially supported by U.S. Department of Energy grants DE-SC0008270 and DE-SC0014085, and U.S. National Science Foundation (NSF) grants EF 1137293 and OIA-1301789. The work of Ying Wang was partially supported by the NSF grant DMS-1720489. All authors declare no conflict of interest on this work.

References

- Ahlström, A., Smith, B., Lindström, J., Rummukainen, M., & Uvo, C. B. (2013). GCM characteristics explain the majority of uncertainty in projected 21st century terrestrial ecosystem carbon balance. *Biogeosciences*, *10*, 1517–1528.
- Ahlström, A., Xia, J. Y., Arneeth, A., Luo, Y. Q., & Smith, B. (2015). Importance of vegetation dynamics for future terrestrial carbon cycling. *Environmental Research Letters*, *10*, 054019.
- AmeriFlux. (2016). Retrieved from <http://ameriflux.lbl.gov/>
- Anav, A., Friedlingstein, P., Kidston, M., Bopp, L., Ciais, P., Cox, P., . . . Zhu, Z. (2013). Evaluating the land and ocean components of the global carbon cycle in the CMIP5 earth system models. *Journal of Climate*, *26*, 6801–6803.
- Arora, V., Boer, G. J., Friedlingstein, P., Eby, M., Jones, C. D., Christian, J. R., . . . Wuj, T. (2013). Carbon-concentration and carbon-climate feedbacks in CMIP5 earth system models. *Journal of Climate*, *26*, 5289–5314.
- Ball, J. T., Woodrow, I. E., & Berry, J. A. (1987). A model predicting stomatal conductance and its contribution to the control of photosynthesis under different environmental conditions. In J. Biggens (Ed.), *Progress in photosynthesis research* (pp. 221–224). Zoetermeer, the Netherlands: Martinus Nijhoff.
- Barford, C. C., Wofsy, S. C., Goulden, M. L., Munger, J. W., Pyle, E. H., Urbanski, S. P., . . . Moore, K. (2001). Factors controlling long- and short-term sequestration of atmospheric CO₂ in a mid-latitude forest. *Science*, *294*, 1688–1691.
- Brovkin, V., Boysen, L., Arora, V. K., Boisier, J. P., Cadule, P., Chini, L., . . . Weiss, M. (2013). Effect of anthropogenic land-use and land-cover changes on climate and land carbon storage in CMIP5 projections for the twenty-first century. *Journal of Climate*, *26*, 6859–6881.
- Carvalhais, N., Forkel, M., Khomik, M., Bellarby, J., Jung, M., Migliavacca, M., . . . Reichstein, M. (2014). Global covariation of carbon turnover times with climate in terrestrial ecosystems. *Nature*, *514*, 213–217.
- Cox, P. M., Pearson, D., Booth, B. B., Friedlingstein, P., Huntingford, C., Jones, C. D., & Luke, C. M. (2013). Sensitivity of tropical carbon to climate change constrained by carbon dioxide variability. *Nature*, *494*, 341–344.
- Farquhar, G. D., von Caemmerer, S., & Berry, J. A. (1980). A biochemical model of photosynthetic CO₂ assimilation in leaves of C₃ species. *Planta*, *149*, 78–90.
- Fisher, J. B., Huntzinger, D. N., Schwalm, C. R., & Sitch, S. (2014). Modeling the terrestrial biosphere. *Annual Review of Environment and Resources*, *39*, 91–123.
- Friedlingstein, P., Cox, P., Betts, R., Bopp, L., von Bloh, W., Brovkin, V., . . . Zeng, N. (2006). Climate-carbon cycle feedback analysis: Results from the C⁴MIP model intercomparison. *Journal of Climate*, *19*, 3337–3353.
- Friedlingstein, P., Meinshausen, M., Arora, V. K., Jones, C. D., Anav, A., Liddicoat, S. K., & Knutti, R. (2014). Uncertainties in CMIP5 climate projections due to carbon cycle feedbacks. *Journal of Climate*, *27*, 511–526.
- Friend, A. D., Lucht, W., Rademacher, T. T., Keribin, R., Betts, R., Cadule, P., . . . Ian Woodward, F. (2014). Carbon residence time dominates uncertainty in terrestrial vegetation responses to future climate and atmospheric CO₂. *Proceedings of the National Academy of Sciences of the United States of America*, *111*, 3280–3285.
- Hararuk, O., & Luo, Y. Q. (2014). Improvement of global litter turnover rate predictions using a Bayesian MCMC approach. *Ecosphere*, *5*, 163.
- Hararuk, O., Xia, J. Y., & Luo, Y. Q. (2014). Evaluation and improvement of a global land model against soil carbon data using a Bayesian Markov chain Monte Carlo method. *Journal of Geophysical Research: Biogeosciences*, *119*, 403–417. <https://doi.org/10.1002/2013JG002535>

- He, Y. J., Trumbore, S. E., Torn, M. S., Harden, J. W., Vaughn, L. J. S., Allison, S. D., & Randerson, J. T. (2016). Radiocarbon constraints imply reduced carbon uptake by soils during the 21st century. *Science*, *353*, 1419–1924.
- Jiang, L., Yan, Y., Hararuk, O., Mickle, N., Xia, J., Shi, Z., . . . Luo, Y. (2015). Scale-dependent performance of CMIP5 Earth system models in simulating terrestrial vegetation carbon. *Journal of Climate*, *28*, 5217–5232.
- Jones, C., Robertson, E., Arora, V., Friedlingstein, P., Shevliakova, E., Bopp, L., . . . Tjiputra, J. (2013). Twenty-first-century compatible CO₂ emissions and airborne fraction simulated by CMIP5 Earth system models under four representative concentration pathways. *Journal of Climate*, *26*, 4398–4413.
- Le Quéré, C., Moriarty, R., Andrew, R. M., Peters, G. P., Ciais, P., Friedlingstein, P., . . . Zeng, N. (2015). Global carbon budget 2014. *Earth System Science Data*, *7*, 47–85. <https://doi.org/10.5194/essd-7-47-2015>
- Lichter, J., Barron, S. H., Bevacqua, C. E., Finzi, A. C., Irving, K. F., Stemmler, E. A., & Schlesinger, W. H. (2005). Soil carbon sequestration and turnover in a pine forest after six years of atmospheric CO₂ enrichment. *Ecology*, *86*, 1835–1847.
- Luo, Y., Ahlström, A., Allison, S. D., Batjes, N. H., Brovkin, V., Carvalhais, N., . . . Zhou, T. (2016). Toward more realistic projections of soil carbon dynamics by Earth system models. *Global Biogeochemical Cycles*, *30*, 40–56. <https://doi.org/10.1002/2015GB005239>
- Luo, Y. Q., Keenan, T. F., & Smith, M. (2015). Predictability of the terrestrial carbon cycle. *Global Change Biology*, *21*, 1737–1751.
- Luo, Y. Q., Shi, Z., Lu, X., Xia, J., Liang, J., Jiang, J., . . . Wang, Y.-P. (2017). Transient dynamics of terrestrial carbon storage: Mathematical foundation and its applications. *Biogeosciences*, *14*, 145–161.
- Luo, Y. Q., & Weng, E. S. (2011). Dynamic disequilibrium of terrestrial carbon cycle under global change. *Trends in Ecology & Evolution*, *26*, 96–104.
- Manzoni, S., & Porporato, A. (2009). Soil carbon and nitrogen mineralization: Theory and models across scales. *Soil Biology and Biochemistry*, *41*, 1355–1379.
- McCarthy, H. R., Oren, R., Finzi, A. C., & Johnsen, K. H. (2006). Canopy leaf area constrains [CO₂]-induced enhancement of productivity and partitioning among aboveground carbon pools. *Proceedings of the National Academy of Sciences of the United States of America*, *103*, 19356–19361.
- McCarthy, H. R., Oren, R., Johnsen, K. H., Gallet-Budynek, A., Pritchard, S. G., Cook, C. W., . . . Finzi, A. C. (2010). Re-assessment of plant carbon dynamics at the Duke free-air CO₂ enrichment site: Interactions of atmospheric [CO₂] with nitrogen and water availability over stand development. *New Phytologist*, *185*, 514–528.
- Melillo, J. M., Butler, S., Johnson, J., Mohan, J., Steudler, P., Lux, H., . . . Tang, J. (2011). Soil warming, carbon-nitrogen interactions, and forest carbon budgets. *Proceedings of the National Academy of Sciences of the United States of America*, *108*, 9508–9512.
- Oleson, K., Lawrence, D. M., Bonan, G. B., Drewniak, B., Huang, M., Koven, C. D., . . . Yang, Z.-L. (2013). *Technical description of version 4.5 of the Community Land Model (CLM)*. Boulder, CO: National Center for Atmospheric Research.
- Peng, J., Dan, L., & Huang, M. (2014). Sensitivity of global and regional terrestrial carbon storage to the direct CO₂ effect and climate change based on the CMIP5 model intercomparison. *PLoS ONE*, *9*, e95282.
- Qian, T. T., Dai, A. G., Trenberth, K. E., & Oleson, K. W. (2006). Simulation of global land surface conditions from 1948 to 2004. Part I: Forcing data and evaluations. *Journal of Hydrometeorology*, *7*, 953–975.
- Shi, Z., Xu, X., Hararuk, O., Jiang, L., Xia, J., Liang, J., . . . Luo, Y. (2015). Experimental warming altered rates of carbon processes, allocation, and carbon storage in a tallgrass prairie: A data assimilation approach. *Ecosphere*, *6*, Article 210.
- Sierra, C. A., & Müller, M. (2015). A general mathematical framework for representing soil organic matter dynamics. *Ecological Monographs*, *85*, 505–524.
- Sitch, S., Huntingford, C., Gedney, N., Levy, P. E., Lomas, M., Piao, S. L., . . . Woodward, F. I. (2008). Evaluation of the terrestrial carbon cycle, future plant geography and climate-carbon cycle feedbacks using five Dynamic Global Vegetation Models (DGVMs). *Global Change Biology*, *14*, 2015–2039.
- Tian, H. Q., Lu, C., Yang, J., Banger, K., Huntzinger, D. N., Schwalm, C. R., . . . Zeng, N. (2015). Global patterns and controls of soil organic carbon dynamics as simulated by multiple terrestrial biosphere models: Current status and future directions. *Global Biogeochemical Cycles*, *29*, 775–792. <https://doi.org/10.1002/2014GB005021>
- Todd-Brown, K. E. O., Randerson, J. T., Hopkins, F., Arora, V., Hajima, T., Jones, C., . . . Allison, S. D. (2014). Changes in soil organic carbon storage predicted by Earth system models during the 21st century. *Biogeosciences*, *11*, 2341–2356.
- Todd-Brown, K. E. O., Randerson, J. T., Post, W. M., Hoffman, F. M., Tarnocai, C., Schuur, E. A., & Allison, S. D. (2013). Causes of variation in soil carbon predictions from CMIP5 Earth system models and comparison with observations. *Biogeosciences*, *10*, 1717–1736.
- Urbanski, S., Barford, C., Wofsy, S., Kucharik, C., Pyle, E., Budney, J., . . . Munger, J. W. (2007). Factors controlling CO₂ exchange on timescales from hourly to decadal at Harvard Forest. *Journal of Geophysical Research*, *112*, G02020. <https://doi.org/10.1029/2006JG000293>
- Wang, W. L., Dungan, J., Hashimoto, H., Michaelis, A. R., Milesi, C., Ichii, K., & Nemani, R. R. (2011). Diagnosing and assessing uncertainties of terrestrial ecosystem models in a multimodel ensemble experiment: 2. Carbon balance. *Global Change Biology*, *17*, 1367–1378.
- Wang, Y. P., & Leuning, R. (1998). A two-leaf model for canopy conductance, photosynthesis and partitioning of available energy. Part I: Model description and comparison with a multi-layered model. *Agricultural and Forest Meteorology*, *91*, 89–111.
- Weng, E. S., & Luo, Y. Q. (2008). Soil hydrological properties regulate grassland ecosystem responses to multifactor global change: A modeling analysis. *Journal of Geophysical Research*, *113*, G03003. <https://doi.org/10.1029/2007JG000539>
- Wieder, W. R., Cleveland, C. C., Smith, W. K., & Todd-Brown, K. (2015). Future productivity and carbon storage limited by terrestrial nutrient availability. *Nature Geoscience*, *8*, 441–444.
- Xia, J. Y., Luo, Y. Q., Wang, Y. P., & Hararuk, O. (2013). Traceable components of terrestrial carbon storage capacity in biogeochemical models. *Global Change Biology*, *19*, 2104–2116.